



Dimensionality differences between sticky and non-sticky chaotic trajectory segments in a 3D Hamiltonian system

K. Tsiganis^{a,*}, A. Anastasiadis^b, H. Varvoglis^a

^a *Section of Astrophysics, Astronomy and Mechanics, Department of Physics, University of Thessaloniki, GR-540 06, Thessaloniki, Greece*

^b *National Observatory of Athens, Institute for Space Applications and Remote Sensing, Palea Penteli, GR-152 36, Greece*

Accepted 28 July 1999

Abstract

Chaotic trajectories in Hamiltonian systems may have a peculiar evolution, owing to stickiness effects or migration to adjacent stochastic regions. As a result, the function $\chi(t)$, which measures the exponential divergence of nearby trajectories, changes its behaviour within different time intervals. We obtain such trajectories, through numerical integration, for a model 3D Hamiltonian system. Having the plots of $\chi(t)$ as a guide, we divide trajectories into segments, each one being assigned an Effective Lyapunov Number (ELN), λ_i . We monitor the evolution of the trajectories through a “quasi-integral” time series, which can follow *trapping* or *escape* events. Using the time-delay reconstruction scheme, we calculate the correlation dimension, $D^{(2)}$, of each trajectory segment. Our numerical results show that, as the ELN of different segments increases, the correlation dimension of the set on which the trajectory segment is embedded, also tends to increase by a statistically significant amount. This result holds only if the differences of the ELN are relatively large, reflecting motion within different phase-space domains, indicating that the transport process does not have the same statistical properties throughout the phase space. As a consequence, $D^{(2)}$ can serve as a scalar index to discriminate between regions of stickiness and regions of unimpeded transport. © 2000 Elsevier Science Ltd. All rights reserved.

1. Introduction – Motivation

In the past few years, a lot of work has been done towards a possible connection between the maximal Lyapunov Characteristic Number (LCN),

$$\lambda = \lim_{t \rightarrow \infty} \chi(t) = \lim_{t \rightarrow \infty} \left[\frac{1}{t} \ln \frac{d(t)}{d(0)} \right], \quad (1)$$

and transport in the phase space of Hamiltonian systems (see e.g. [1–5]). In practice, different chaotic trajectories may have different λ 's. This, in general, means that the phase space regions spanned by different trajectories may be separated by some kind of “barriers” which inhibit transport between them. This phenomenon is common in Hamiltonian systems with two degrees of freedom, where, if the perturbation is not very strong, KAM surfaces that survive the perturbation separate different stochastic layers. However, for an N -degrees-of-freedom ($N \geq 3$) Hamiltonian system, the value of the maximal LCN, being defined by Eq. (1) as the limit of $\chi(t)$ for $t \rightarrow \infty$, should be the same for every chaotic trajectory, due to Arnol'd diffusion [6,7]. Therefore, in the case of moderate perturbation, the maximal LCN is insufficient to describe transport phenomena in such systems, since it does not provide any information

* Corresponding author.

E-mail address: tsiganis@astro.auth.gr (K. Tsiganis).

about the different parts of the phase space in which trajectories may remain for considerable time intervals.

For moderate values of the perturbation, the topology of the phase space is very complex. Families of invariant sets that persist under the perturbation, being also surrounded by the “ghosts” of those who are not completely destroyed, called *cantori* [8,9], form a set of non-zero measure. Chaotic trajectories departing from phase space regions that are mostly stochastic avoid, generically, these “quasi-barriers” [5–10]. An explanation for that is given in [11] (see also [12]) by the shape of the lobes formed by the asymptotic curves in the vicinity of the principal cantorous. However, since the set of cantori surrounding a stable orbit has zero measure, it is possible for a chaotic trajectory to enter the “quasi-barrier” and *stick* close to a stable orbit. The same mechanism would now prevent the trajectory from escaping. This would, of course, result in a decrease of $\chi(t)$. The evolution inside the region of a “quasi-barrier” also follows the above scenario, so that a trapped chaotic trajectory may bounce from the vicinity of one stable orbit to another, undergoing a peculiar random-walk [13,14], before it manages to exit the “quasi-barrier”, upon which $\chi(t)$ increases again. It is easy to understand that $\chi(t)$ may not saturate in any finite time, if a chaotic trajectory evolves in a way similar to the one described above.

Overlooking the problem of infinite computation time, one usually assigns to the maximal LCN of a chaotic trajectory the value of $\chi(t_{\text{int}})$, where t_{int} is the integration time. However, this is based on the assumption that the character of chaotic motion will not change for $t > t_{\text{int}}$, thus ignoring the phenomena described above. In search of a more operational tool for measuring the degree of stochasticity of trajectories, variants of *finite time Lyapunov exponents* have been introduced by several authors (e.g. [15–19]). In [10] an Effective Lyapunov Number (hereafter ELN) was used as an indicator to discriminate between *trajectory segments* of different behaviour. Using the graph of $\chi(t)$ a trajectory is divided into a number of consecutive segments of duration Δt_i , according to the behaviour of the function $\chi(t)$. The end of a segment is defined as the time t_i at which $\chi(t)$ tends to saturate to a definite value, or an abrupt change in the monotony of $\chi(t)$ occurs. In the latter case one implicitly assumes that $\chi(t)$ has also saturated, but for a short time. The ELN (or Local LCN as was originally called) of the segment is then given by the value $\lambda_i = \chi(t_i)$.

ELNs, as defined above, do have a physical meaning; they are connected to the “memory” of the system in the specific phase-space region that the trajectory spans during the respective time interval. If a trajectory can be divided into segments with different ELNs this is an indication that it has visited several phase-space regions. Although fluctuations of the function $\chi(t)$ do not necessarily mean migration to an adjacent phase-space domain, it was shown in [10] that trajectory segments which are associated to a *monotonic increase* of $\chi(t)$, result in a steep increase of the cumulative phase-space volume visited by the trajectory up to time t . On the other hand, a monotonically decreasing phase of $\chi(t)$, which may follow the increasing segment, produces only a small variation of the cumulative volume, indicating that the trajectory returns to an already visited domain, probably following a slightly different path.

In order to distinguish between *sticky* and *non-sticky* chaotic orbits one may simply use a Poincaré surface of section. However, in the case of three- (or more) degrees-of-freedom Hamiltonian systems one cannot visualize a Poincaré section. An alternative way to monitor the evolution of a trajectory, which we are using in this paper, is by inspecting a “quasi-integral” time series, uniquely defined for a given set of initial conditions; this is a common practice in celestial mechanics. The statistical properties of a “quasi-integral” time series should be very different between regular and stochastic trajectories. On the other hand, if a trajectory is *sticky*, the statistical properties of the time series may not be very different from those of a regular trajectory. Moreover, if a sticky orbit manages to escape from the “quasi-barrier”, migrating towards a more stochastic phase-space region, the statistical properties of the time series’ subpart which corresponds to the new trajectory segment, may also differ from those of the previous segment.

In this paper, we use both $\chi(t)$ plots (and ELNs) and a suitable “quasi-integral” time series to study the dynamics of trajectories taken from a 3D Hamiltonian system. Using the $\chi(t)$ plots, we split the trajectories into segments. With the “quasi-integral” time series we try to distinguish between fluctuations of the ELN which imply migration of the trajectory to a new phase-space region, and also changes in the statistical properties of the time series, from those which do not. This is done by calculating the *correlation dimension*, $D^{(2)}$, of each time series’ subpart which corresponds to a given trajectory segment. This is a particularly interesting statistical property of the time series, since it is an invariant measure characterizing the

phase-space subset on which this trajectory segment is embedded. Thus, the value of $D^{(2)}$ can be used to quantify possible differences in the multifractal character of the dynamics between (i) regions where chaotic motion is geometrically confined for long (but finite) times by imperfect barriers and (ii) phase-space regions of unimpeded transport.

It is known that Hamiltonian systems generate *fat fractals* [20]. This means that the dynamics have multifractal properties but, in the limit of infinite time, the Hausdorff dimension of the set on which a chaotic trajectory is embedded is an integer number, namely $D_H = 2N - i$, where $2N$ is the dimension of the phase space, and $i \leq N$ is the number of isolating integrals of motion that are globally preserved under the perturbation. Accordingly, for a periodic orbit $D_H = N$. A sticky trajectory, on the other hand, is forced to remain close to a stable orbit, by the mechanism described above, thus behaving locally in a more regular manner. The ELN of the segment corresponding to the time spent in the *trap* should be small. It is reasonable to assume that the dimension of the embedding set also should not be very different from the one which corresponds to a stable orbit. On the other hand, away from “quasi-barriers”, ELN should increase and we expect the same for the dimension too.

If the above considerations are true, the statistical properties of the process, by which chaotic trajectories tend to fill the available space, is not the same throughout the phase space, but are dictated by the measure of KAM curves contained within a phase-space region. As the ELNs of trajectory segments get larger, the dimensionality of the corresponding embedding set should also increase, provided that the different ELNs imply motion within different phase-space domains and not *jumps* between the overlapping chaotic strips of a “quasi-barrier”. As a consequence, the value of the correlation dimension could be used to distinguish between sticky trajectories and chaotic trajectories which evolve away from “quasi-barriers”.

In the next section we introduce the Hamiltonian model and describe the techniques used for dimension estimates. Our results are presented in Section 3. The last part of this paper, Section 4, is devoted to conclusions and discussion.

2. Model and techniques

We study trajectories in a well known 3D Hamiltonian system [21–23] which describes three non-linearly coupled oscillators. The Hamiltonian per unit mass is of the form

$$H = \frac{1}{2}(p_x^2 + p_y^2 + p_z^2) + \frac{1}{2}Ax^2 + \frac{1}{2}By^2 + \frac{1}{2}Cz^2 - \epsilon xz^2 - \eta yz^2 = h, \quad (2)$$

where the first four terms correspond to the Hamiltonian, H_0 , of the integrable non-coupled system. The parameters were set at $A = 0.9$, $B = 0.4$, $C = 0.225$, $\epsilon = 0.56$, $\eta = 0.2$ and $h = 0.00765$ in all our experiments. For this set of values the phase space contains two chaotic domains, of different volume, which communicate (for a detailed discussion on the phase space structure see [21–23]). The canonical equations are integrated using a fourth order Runge–Kutta integrator with adaptive stepsize control [24], for various initial conditions in the x – y plane ($z = 0$), with $p_x(0) = p_y(0) = 0$. The accuracy parameter was set to 0.5×10^{-15} and the consistency of the energy integral was checked. We follow a standard numerical technique for the calculation of the maximal LCN (see e.g. [25]), integrating simultaneously two trajectories, one “central” and one “nearby”, differing in x_0 by $\Delta x = 10^{-7}$ and in $p_{z,0}$ by Δp_z , as calculated through the energy integral. Phase space projections on the z – p_z plane and t – $\chi(t)$ plots for different types of trajectories are shown in Figs. 1–5. For all the trajectories examined, we stop the integration after $t_{\text{int}} = 1.5 \times 10^6$.

When ϵ and η are non-zero, H_0 is no longer a constant of motion and one can construct the so-called “quasi-integral” time series $H_0(t_i)$ ($i = 1, 2, \dots, n$), which is uniquely defined for any given set of initial conditions. Figs. 1–5 also show the corresponding t – $H_0(t)$ graphs for the five trajectories mentioned. By comparing the $H_0(t_i)$ plots with the corresponding ones for $\chi(t)$, one can observe that, in the cases where $\chi(t)$ shows relatively large variations, the behaviour of the $H_0(t_i)$ time series also changes. In particular, the maximum amplitude of oscillation of $H_0(t_i)$, as well as the distribution of spikes of different magnitudes contained in the graph, change significantly.

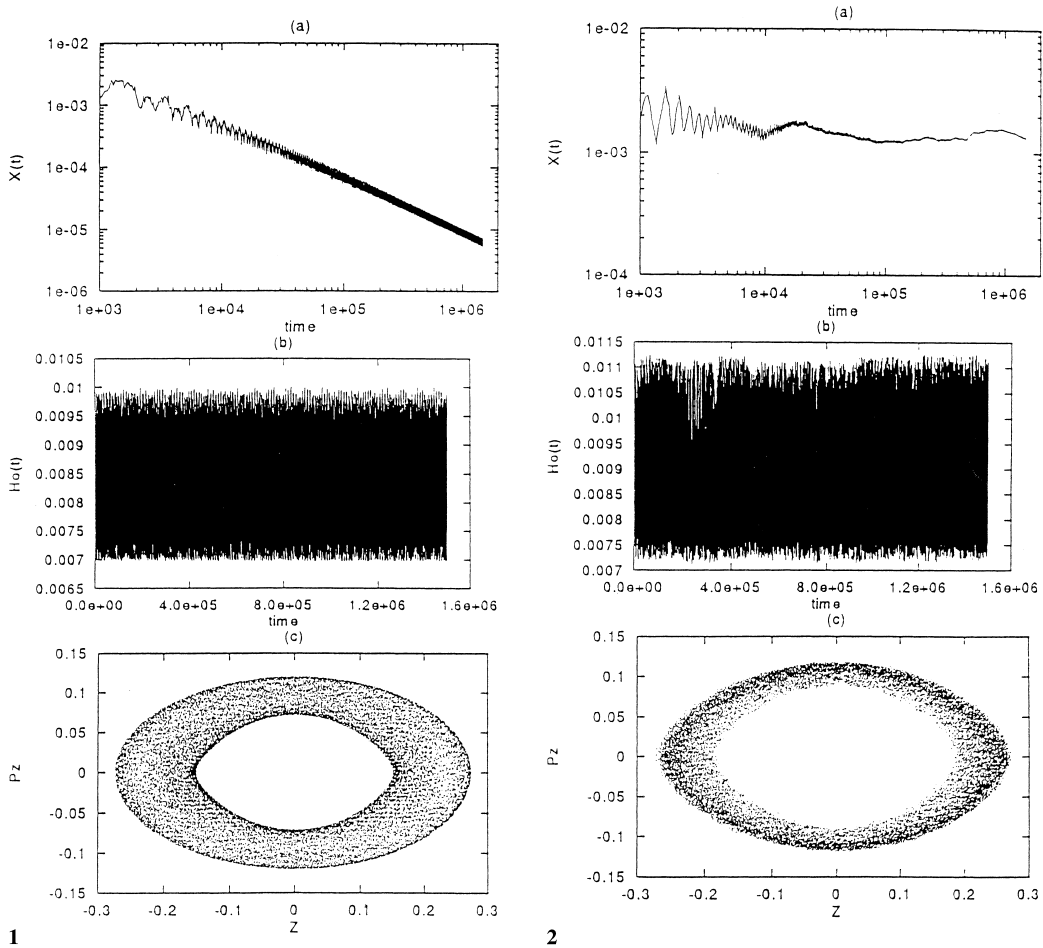


Fig. 1. (a) $t-\chi(t)$ plot, (b) the $H_0(t)$ timeseries and (c) $z-p_z$ projection for $x_0 = 0.009, y_0 = 0.02625$.

Fig. 2. (a) $t-\chi(t)$ plot, (b) the $H_0(t)$ timeseries and (c) $z-p_z$ projection for $x_0 = -0.045, y_0 = 0.02$.

We quantify the differences between the trajectory segments by calculating the correlation dimension, $D^{(2)}$, from the time series subpart that corresponds to each segment. The q -order generalized dimensions, which constitute the $D^{(q)}$ -spectrum, are invariant quantities which give important geometrical and topological information about the phase space set (actually the measure defined on it) on which the trajectory is embedded. In particular, the $q = 0$ case, called *capacity dimension*, is an approximation to the Hausdorff dimension of this set (i.e. the support of the measure). If there were differences in the value of $D^{(0)}$ between sticky and non-sticky chaotic trajectories this would mean that the transport process takes place, effectively, on a subspace of different dimensionality. If the dynamics have multifractal properties, something which is known for Hamiltonian systems, the rest of the generalized dimensions (actually the $q = 1$ and $q = 2$ cases) are equally, if not more, important. The $q = 1$ case, called *information dimension*, characterizes the non-uniformity of the measure. It actually measures how the average information needed to specify a point x with accuracy ϵ scales with ϵ . Due to its relation to the Shannon information (see [31]) $D^{(1)}$ is the most significant dimension for a multifractal measure. The correlation dimension ($q = 2$) measures how correlations between points that lie within a neighborhood of size ϵ scales with ϵ . As the $D^{(q)}$ -spectrum is a non-increasing function of q , $D^{(2)}$ can be considered as a lower bound for $D^{(1)}$. Moreover, the definition of $D^{(2)}$ ensures a much smaller error in its estimation from a limited set of data and, therefore, makes $D^{(2)}$ the most reliable – $D^{(2)}$ is the one used in most applications. A detailed description of the set generated in phase space and the appropriate measure defined on it would consist of calculating the whole $D^{(q)}$ -spectrum and quantifying the differences between the spectra of sticky and non-sticky chaotic trajectories. This is however beyond the scopes of the present paper.

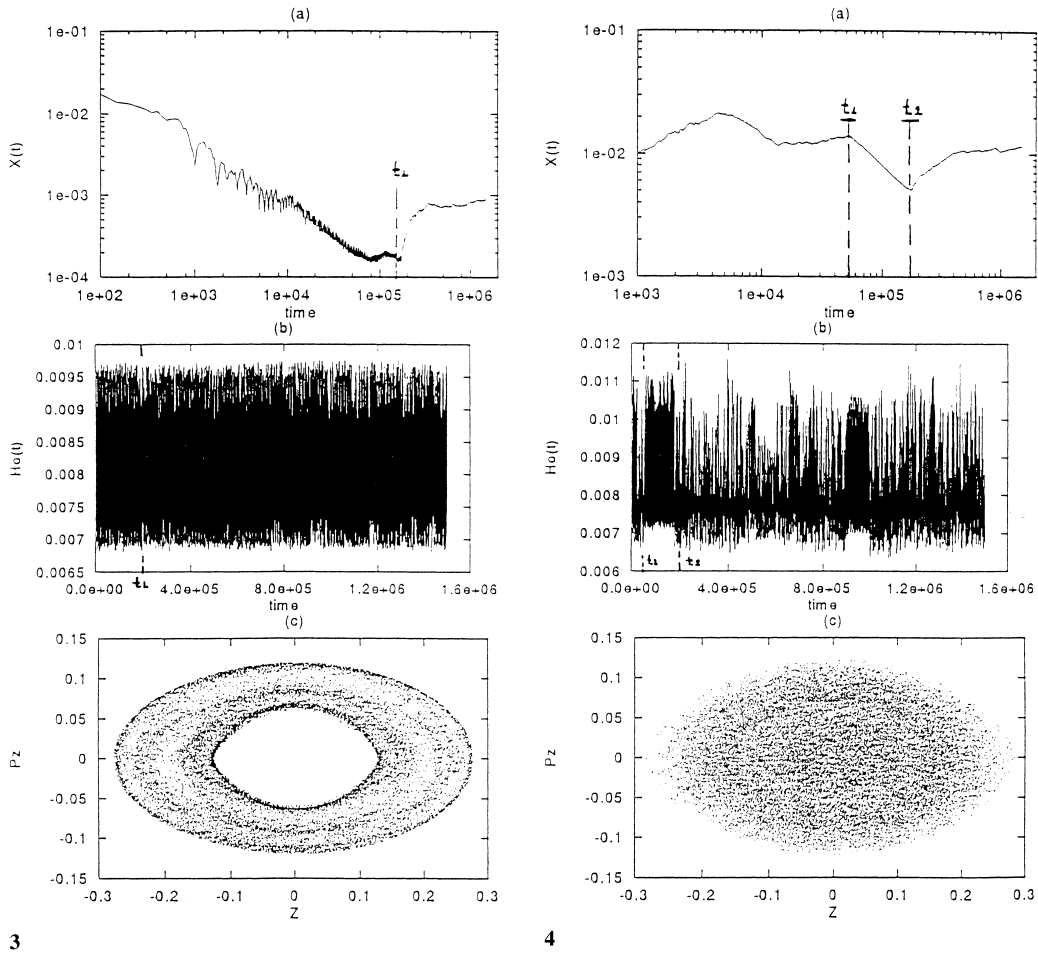


Fig. 3. (a) $t-\zeta(t)$ plot, (b) the $H_0(t)$ timeseries and (c) $z-p_z$ projection for $x_0 = 0.01725, y_0 = 0.032$.
 Fig. 4. (a) $t-\zeta(t)$ plot, (b) the $H_0(t)$ timeseries and (c) $z-p_z$ projection for $x_0 = 0.1, y_0 = 0.0633$.

The correlation dimension $D^{(2)}$ is given by the logarithmic slope of the correlation integral $C_2(r)$,

$$D^{(2)} = \lim_{r \rightarrow 0} \frac{d(\log C_2(r))}{d(\log r)}, \tag{3}$$

where $C_2(r)$ is calculated through the formula [28]

$$C_2(r) = \frac{1}{N_p} \sum_{i=1}^{N_p} \left[\frac{1}{Z} \sum_{|i-j|>W} \Theta(r - |\vec{x}_i - \vec{x}_j|) \right], \tag{4}$$

where \vec{x}_i, \vec{x}_j are phase space vectors, W is the autocorrelation time of the trajectory, N_p the number of points used, Z a normalization parameter, $\Theta(x)$ the Heaviside step function, and r is the radius of a n -dimensional hypersphere centered at \vec{x}_i , where n is the dimension of the state space. The restriction $|i - j| > W$ excludes all \vec{x}_j 's that are time-correlated with \vec{x}_i , as they would affect the estimate of the geometrical (spatial) structure of the set. Since we are interested in comparing the resulting $D^{(2)}$ values for different trajectory segments, the same number of points N_p has to be used in all of the estimates.

$C_2(r)$ can also be calculated using the time series of any analytic function of the system's variables. Takens [26] was the first to prove that one can reconstruct certain properties of the n -dimensional state space of a dynamical system by properly constructing a new vector space from a time series, provided that

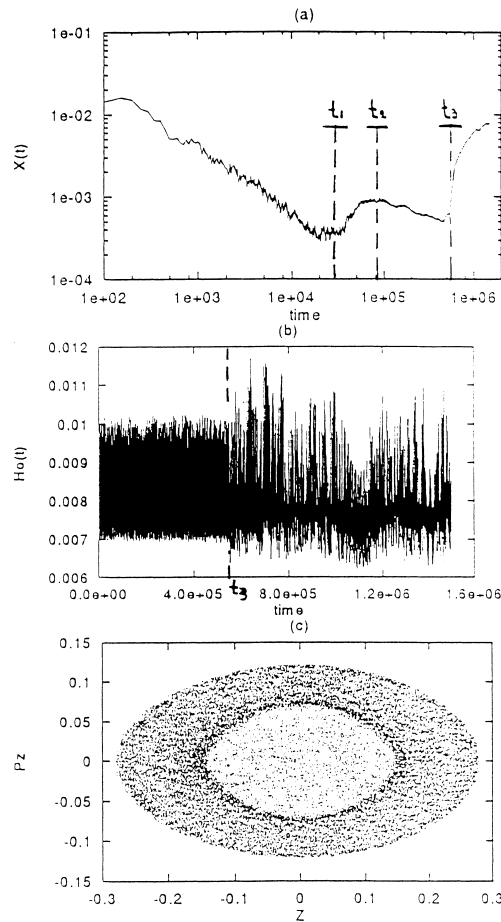


Fig. 5. (a) $t-\chi(t)$ plot, (b) the $H_0(t)$ timeseries and (c) $z-p_z$ projection for $x_0 = 0.0095, y_0 = 0.0415$.

the metric properties of the original space are conserved. The method of creating the vectors of the reconstructed space, $\vec{y}(t_i)$, from a given time series, $Y(t_i)$, is known as the *time-delay reconstruction scheme*. For a time instant t_i , the vector \vec{y}_i is given by

$$\vec{y}_i = [Y(t_i), Y(t_i + \tau), Y(t_i + 2\tau), \dots, Y(t_i + (d_e - 1)\tau)], \tag{5}$$

where τ is a properly defined time-delay parameter and d_e is the (embedding) dimension of the Takens space. It is crucial that $d_e \geq (2D + 1)$, where D is the dimension of the underlying object, in order to achieve an embedding (in our case $D \leq 5$). An extensive discussion on *embedology* is given in [27]. The use of the time-delay scheme requires an involved procedure in defining the *embedding parameters*, i.e. the delay time, τ , and the embedding dimension, d_e , as well as the minimum number of points needed, N_p . Practical details concerning this subject can be found, for example, in [28] or [29]. We just mention at this point that the number of points used in our calculations, N_p , is indeed adequate for reliable estimates of $D^{(2)}$, in all of our cases. The choice of N_p was based on the results of [30], according to which the ratio $m = (N_p \Delta t)/W$, where t is the time interval between two successive points, should be at least $m > 50$. This also depends on the value of the dimension of the underlying object. In our case $D^{(2)}$ is definitely less than $2n - 1 = 5$, where $n = 3$ is the number of degrees of freedom, and m , according to the results of [30], should be of the order of 100 or greater. In all the segments studied in this paper we were able to go up to $m = 200$. For extended discussions on non-linear time series analysis techniques, the reader is referred to Ref. [31].

As mentioned above, any analytic function of the variables can be used for a correlation dimension estimate. We selected $H_0(t_i)$ having in mind a possible analogy with specific astronomical problems. In

particular, when integrating trajectories in a given model for asteroidal motion, the orbital elements associated with the Delaunay actions are usually recorded as time series, which are also “quasi-integrals”. Migration of an asteroid after $t = T_E$ to a more chaotic region of the phase space is then visualized by much wilder oscillations present in the time series. Such an event is also seen, and recorded by $H_0(t_i)$, in our model. Therefore, it is reasonable to expect that the results for $H_0(t_i)$ in the present model should be applicable in the case of other “quasi-integral” time series as well.

Another important issue that one has to keep in mind, when working with time series, is the concept of stationarity, i.e. the independency of its statistical properties with respect to absolute time. For a deterministic process, as in our case, this is always true except for possible *transition phases*, for which any finite value of $D^{(2)}$ found will be meaningless [32]. In this paper we use a stationarity test proposed by Isliker and Kurths [32], based on a numerical estimation of the invariant measure.

3. Results

In this section we present numerical results concerning trajectories of different types. After discussing the phenomenology of the evolution of these trajectories, and defining the appropriate number of segments, we present the results of the $D^{(2)}$ estimates for these segments.

3.1. Phenomenology

Fig. 1 presents the z - p_z projection, t - $\chi(t)$ and t - $H_0(t)$ plots for a *regular* trajectory. The function $\chi(t)$ is monotonically decreasing with time, and it would reach zero at infinite time, if the trajectory is to remain regular. However, keeping in mind the discussion included in the introduction, our knowledge about the time evolution of any trajectory goes as far as the integration time. Since we cannot be sure whether the trajectory will indeed remain regular, it is safer to say that this may be a segment belonging to a sticky trajectory but, for this time interval, the upper bound for the ELN is $\lambda \approx 5 \times 10^{-6}$. In the z - p_z plane the trajectory remains in a “ring” structure for all times. Although a phase space projection does not provide a lot of physically meaningful information, unlike a surface of section, it is sometimes useful in distinguishing between the parts of the phase space in which different types of trajectories evolve (this will become more clear in the following paragraphs). We label the part of the z - p_z plane covered by this ring as *region A*. Finally, the $H_0(t)$ time series has the shape of a low amplitude oscillating function, which seems almost periodic. The stationarity test was successful, so that any subpart is apt for correlation dimension estimates.

The trajectory in Fig. 2 shows a completely different character than the previous one. The evolution of $\chi(t)$ is typical of a chaotic trajectory, saturating *quickly* to a positive ELN value, $\lambda \approx 1.4 \times 10^{-3}$. One can claim, of course, that saturation is a matter of interpretation. A strict definition of saturation may be used, e.g. by demanding that the slope of the observed plateau, as measured by a least-squares fit, is equal to zero, within a desired significance level. However, if relatively long segments of monotonic increase (or decrease) of $\chi(t)$ are not present in the graph, we do not think that one should complicate things more than necessary. In the projection plot, the occupied “ring” on the z - p_z plane has smaller width than the one in Fig. 1, indicating that the two trajectories do not span the same phase-space region (we label this thinner “ring” as *region B*). $H_0(t_i)$ is characterized by erratic excursions, in contrast to the quasiperiodic behaviour of Fig. 1(b). In spite of the appearance of some narrow gaps in the $H_0(t_i)$ plot at $t \approx 3.5 \times 10^5$, which correspond to a small hump seen in the $\chi(t)$ plot, the stationarity test was successful again.

The last three trajectories are the most interesting for the purpose of this paper. The trajectory presented in Fig. 3 seems initially regular, as $\chi(t)$ is decreasing. After $t_1 \approx 1.8 \times 10^5$, $\chi(t)$ saturates to an ELN value of $\lambda_1 \approx 1.6 \times 10^{-4}$, before it starts to rise again, reaching a plateau of $\lambda_2 \approx 8.9 \times 10^{-4}$ at $t_2 = t_{\text{int}}$. This evolution is indicative of trapping in a sticky domain where, after $t = t_1$, escape to a somewhat more chaotic region is visualised. An interesting feature in this plot is a small peak of $\chi(t)$ around $t \approx 10^5$. This indicates that the trajectory may have entered temporarily in a slightly more stochastic region of the “quasi-barrier” and returned to the previous chaotic region, instead of proceeding to the next one as discussed in [10]. Fig. 3(c) shows again a “ring” structure which is very similar to the one seen in Fig. 1(c). It is, however, a little wider in p_z and it looks distorted, compared to the one formed by the regular trajectory of Fig. 1, as it should be for a

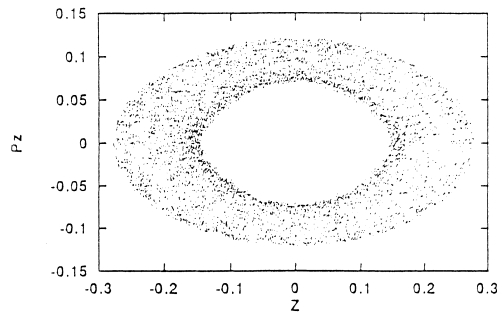


Fig. 6. The z - p_z projection for $t \leq t_3$, $x_0 = 0.0095$, $y = 0.0415$.

sticky trajectory which winds around the stable orbits contained in region A . Looking at $H_0(t)$, Fig. 3(b), we cannot distinguish between the two segments. The importance of this observation will become more evident in the following paragraphs. The stationarity test did not yield any problems in neither segment.

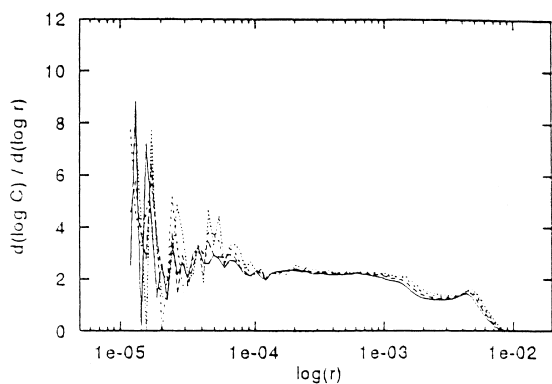
The trajectory in Fig. 4 can be split into three segments. In the beginning, $\chi(t)$ is fluctuating around the value $\lambda_1 \approx 1.4 \times 10^{-2}$. After $t_1 \approx 5.5 \times 10^4$ the trajectory obviously sticks to some “quasi-barrier” and $\chi(t)$ drops down to the value $\lambda_2 \approx 5.1 \times 10^{-3}$ at $t_2 \approx 1.8 \times 10^5$. Finally, after t_2 , the orbit escapes from the “trap”, reaching again an ELN value of $\lambda_3 \approx 1.2 \times 10^{-2}$ at $t = t_{\text{int}}$. The z - p_z projection is much different from the previous orbits. The inner part of the “ring” (hereafter *region C*) is now visited, indicating that this strongly chaotic trajectory occupies a different, and larger, area in the z - p_z plane. $H_0(t_i)$ is characterized by a much more random-looking behaviour. The distinction between the aforementioned three phases can also be seen in the $H_0(t_i)$ graph, as gaps are present at t_1 and t_2 , where the time series changes shape. Again, neither of the three segments had any problems passing the stationarity test.

The last of the trajectories presented here (Fig. 5) has the richest phenomenology. As one can see in Fig. 5(a), the trajectory can be divided into four distinct regimes. From $t = 0$ to $t_1 \approx 3 \times 10^4$ $\chi(t)$ drops with time down to the value $\lambda_1 \approx 3.5 \times 10^{-4}$. This implies that the motion is almost quasiperiodic during this time interval. The second part ($3 \times 10^4 \leq t \leq 8 \times 10^4 = t_2$) is characterized by an increase of $\chi(t)$ up to the value $\lambda_2 \approx 9 \times 10^{-4}$, followed by a much longer part ($8 \times 10^4 \leq t \leq 5 \times 10^5 = t_3$) of a slow decrease of the divergence rate, $\lambda_3 \approx 5.3 \times 10^{-4}$. In the last segment $\chi(t)$ increases steeply, a sign that the trajectory has migrated to another region of the phase space, characterized by a much larger ELN, $\lambda_4 \approx 8 \times 10^{-3}$ at $t = t_{\text{int}}$. The z - p_z projection is similar to the previous one (Fig. 4(c)), since they both fill the inner part of the ring structure seen in the previous projection plots. However, there is a striking difference between Fig. 4(c) and Fig. 5(c) in the detail of the boundaries, as borderlines, similar to the ones which bound region A in Fig. 3(c), are also present in Fig. 5(c). This difference can be understood if one looks at Fig. 6, which is the projection plot taken for $t \leq t_3$, where it is clearly shown that the “filling” of the inner region of the ring (*region C*) does not occur until $t \geq t_3$. This fact is a confirmation that the wilder oscillations of $H_0(t)$, for $t > t_3$, denote migration of the trajectory from one phase space region (A) to another (C).

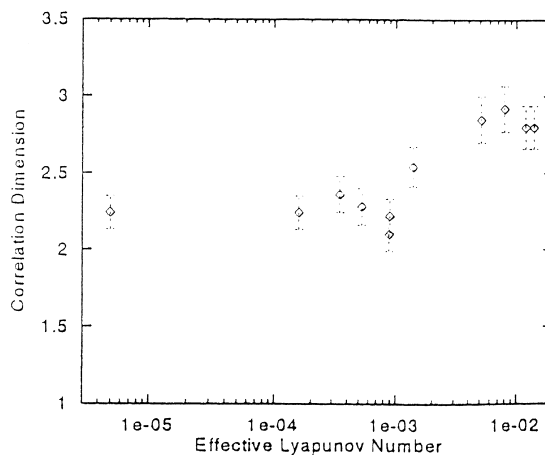
Using the χ^2 -test we verified stationarity for the first three segments of this trajectory. As far as the fourth part is concerned, the stationarity test failed, so that the invariant measure generated by the whole part cannot be reproduced by any subpart of the desired length. In this last part of the trajectory one can distinguish between a *transition phase* ($t_3 \leq t \leq 8 \times 10^5$), where $\chi(t)$ continues to increase steeply, and a *saturation phase* ($t \geq 8 \times 10^5$), where $\chi(t)$ “relaxes”, forming a plateau at $t = t_{\text{int}}$. In the transition phase the stationarity test failed and, hence, the process during this time interval can not be classified within the framework of the present analysis. On the other hand, the test was successful for the part constituting the saturation phase ($t \geq 8 \times 10^5$).

3.2. Dimension estimate

We proceed by performing correlation dimension estimates for all the trajectory segments mentioned. Fig. 7 is a typical “slope plot”, i.e. the derivative of the correlation integral vs. the radius, $\log(r)$. In the graph, different curves corresponding to different embedding dimensions are superimposed. In order to



7



8

Fig. 7. The “slope plot” for Segment V γ .

Fig. 8. Graphic representation of the results presented in Table 1. For segments with $\lambda \geq 10^{-3}$ the correlation dimension increases from ~ 2.3 to ~ 2.9 .

estimate the dimension accurately, one has to define a “plateau” in these graphs, keeping in mind that the result should be, more or less, independent of the embedding dimension and looking at as small radii as the statistical fluctuations allow. After defining the plateau, a least squares fit is performed in order to determine the value of $D^{(2)}$. The results for all the segments are shown in Table 1, where each segment is labeled by a Latin number denoting the trajectory (I–V, using the order at which the trajectories were presented), and a Greek letter (α – δ) numbering the segment, in order of increasing time. The ELN of each segment is also given in Table 1.

Since dimensionality differences are observed, it is important to ensure whether they are statistically significant, or not. Ellner [33] has shown that the error for a Maximum Likelihood Estimate (MLE) of the correlation dimension is given, on a 95% significance level, by

$$\Delta^{(2)} = \frac{1.96 D^{(2)}}{\sqrt{N/2}} \frac{1}{\sqrt{1 - (r_0/r_{\max})^{D^{(2)}}}}, \tag{6}$$

where $D^{(2)}$ is the dimension we measure, N the number of points used, r_0 the radius at which the plateau begins, and r_{\max} is the radius at which $C_2(r)$ saturates to zero.

Fig. 8 is a graphic representation of the results of Table 1. One can immediately see that the trajectory segments which evolve within region A (I, III α , III β , V α , V β and V γ), for which $\lambda \leq 10^{-3}$, yield the same, statistically, values for the correlation dimension, $D^{(2)} \approx 2.3$. On the other hand, the segments during which

Table 1
ELN vs. correlation dimension

Segment no	ELN, λ	$D^{(2)} \pm \Delta^{(2)}$
I	5.0×10^{-6}	2.24 ± 0.11
II	1.4×10^{-3}	2.53 ± 0.13
III α	1.6×10^{-4}	2.24 ± 0.11
III β	8.9×10^{-4}	2.10 ± 0.11
IV α	1.4×10^{-2}	2.80 ± 0.14
IV β	5.1×10^{-3}	2.85 ± 0.15
IV γ	1.2×10^{-2}	2.80 ± 0.14
V α	3.5×10^{-4}	2.36 ± 0.12
V β	9.0×10^{-4}	2.22 ± 0.11
V γ	5.3×10^{-4}	2.28 ± 0.12
V δ	8.0×10^{-3}	2.92 ± 0.15

motion takes place in region C (and for which $\lambda \geq 5 \times 10^{-3}$) have $D^{(2)} \approx 2.9$. This difference in the $D^{(2)}$ values is verified to be statistically significant. Trajectory II is an intermediate case, having $\lambda = 1.4 \times 10^{-3}$ and $D^{(2)} = 2.53 \pm 0.13$. Its error bar overlaps with the one for the segment $V\alpha$. However, the z - p_z projection shows that it moves in a different region (B). Also, note that the value of $D^{(2)}$ for the *regular* trajectory (I) is the same as for the chaotic (but sticky) segments that evolve in the same phase-space region.

4. Conclusions – Discussion

The results presented in the previous section are characteristic of the different types of evolution discussed in the introduction. In particular, a regular trajectory (I) indicates the existence of a family of invariant sets, which acts as a “quasi-barrier”, immersed in the stochastic web. Trajectories III and V are trapped in the “quasi-barrier” (segments $III\alpha, \beta$ and $V\alpha$ – $V\gamma$), visiting several of the overlapping chaotic strips which surround the stable orbits. We have labeled the region occupied by the “quasi-barrier” as region A . On the other hand, trajectories II and IV lie in two distinct, as suggested by the z - p_z projections and their ELN's, stochastic regions (B and C , respectively), possibly separated by the “quasi-barrier”. The fact that trajectory V manages to exit from region A and migrate to region C confirms that these two phase space regions communicate. This is also evident from the fact that trajectory IV also sticks to region A . However, the ELN of segment $IV\beta$ remains relatively high and the trapping period is small, indicating that the trajectory sticks to the outermost part of the “quasi-barrier” (termed as ‘sticky region II’ in [11]) from which it escapes within a short time.

Following the “quasi-integral” time series, $H_0(t_i)$, we are able to detect changes in the dynamics which correspond to trapping or escape events. Moreover, the results presented in the previous section, concerning dimension estimates, are in agreement with the discussion made in the introduction. In particular, the dimension of the phase-space subset on which a *sticky* segment is embedded does not differ from the dimension of the set on which a *regular* orbit lies. On the other hand, for non-sticky chaotic trajectory segments, with *significantly* higher values of ELN, the dimension of the embedding set also tends to increase by a statistically significant amount. The exact values of the ELNs (and the $D^{(2)}$'s) depend, of course, on the specific dynamical system, as well as on the control parameters involved. Since $D^{(2)}$ is a statistical property of the $H_0(t_i)$ time series, the aforementioned result is another indication that the statistical properties of the transport process, which governs the evolution of trajectories, are not the same throughout the phase space. Instead, they are governed by the measure of the remaining KAM curves within a phase-space region, and their *sticky* borders, as has been suggested recently [13,14].

Consequently, $D^{(2)}$ can serve as a measure of ‘*transportability*’ for chaotic orbits, discriminating between phase-space regions where *stickiness* governs the dynamics, and regions of unimpeded transport. The insensitivity that $D^{(2)}$ exhibits towards small variations of the ELN is, in this sense, an advantage. Trajectory V, for example, is divided into four segments according to the graph of $\chi(t)$, but the first three segments, which have different ELNs but span the same phase-space domain, are characterized by the same value of $D^{(2)}$. Performing the stationarity test for the subpart of $H_0(t)$ corresponding to segments $V\alpha$ – $V\gamma$, i.e. $H_0(t_i)$ for $0 \leq t \leq t_3$, we found that it is, as a whole, stationary, and a unique value of $D^{(2)} \approx 2.3$ can be obtained. Conversely, the segment $V\delta$ gives $D^{(2)} \approx 2.9$. Thus, using $D^{(2)}$ as an index, one need not calculate $\chi(t)$ at all, but simply divide the time series into the *minimum possible number of stationary subparts* and calculate the value of the correlation dimension for each of those subparts. However, this tool is not good for distinguishing between *regular* and *sticky* orbits. For this purpose, a combination with other numerical methods, for example calculation of the *power spectrum* of a short part of the time series (see also [18,34]) would be needed.

One of the main problems, concerning asteroidal motion, is to estimate the “event” time, T_E , which is the time for an asteroid to become planet-crosser. Varvoglis and Anastasiadis [5] have shown that a positive correlation between T_E and the Lyapunov time, $T_L (= 1/\lambda)$, can be established from the solution of a diffusion equation, provided that all resonances are overlapping. Murison et al. [3] found numerically the same relation for trajectories in the Elliptic Restricted Three Body Problem, using a perturbing planet *ten times heavier* than Jupiter. This relation is violated by some asteroids, which reside on chaotic orbits but do not become planet-crossers for much longer times than those predicted by the $T_E(T_L)$ relation (522-Helga is

a well known example). Milani and Nobili [35] termed this behaviour *stable chaos* (see also [36]). The results for trajectories II and V in our model demonstrate a similar behaviour: although II has a higher ELN than V for $t < 5 \times 10^5 = T_E$, it does not migrate to region *B*, while V escapes from region *A* to region *B*, exploring a much bigger area of phase space. Hence, it may be the case that asteroids exhibiting stable chaos move in a region restricted by “quasi-barriers”, such that they remain in it for a long time, exploiting a much smaller volume of phase space than they would in the case of unrestricted transport. Given a model that describes asteroidal motion, one can use the method presented in this paper to check whether “quasi-barriers” are indeed present in the neighbourhood of asteroids exhibiting stable chaotic behaviour.

The problem of formulating a statistical description for weakly chaotic Hamiltonian systems, in which regular regions surrounded by stickiness zones cover a large part of the available phase space, is closely related to the definition and calculation of proper transport coefficients. In a recent paper [37] the notion of local transport coefficients (for 2D area-preserving maps) was introduced and their relation to the coefficients calculated through the mean exit times from a given subset of the phase space [38] was shown. These local coefficients come from relaxing the quasi-linear approximation and assuming phase randomization to occur after sufficiently long times. Thus, in regions where regular motion prevails, long-time correlations are also taken into account and, consequently, the value of these local coefficients is decreased. Chaotic orbits characterized by large Lyapunov exponents and, at the same time, long-time correlated action changes were also found recently [39] in a Hamiltonian model describing the motion of asteroids in the Solar system. An attempt to connect the autocorrelation time of the action time series with the escape time from a certain action-space region was also made, without much success. It was then argued that more refined nonlinear tools, like the mutual information or relevant entropy-like quantities (see [31]), have to be considered in order to derive quantitative statistical laws for the ongoing transport process and to connect them with properly defined transport coefficients. Note, however, that the calculation of entropy-like quantities depends on the choice of a partition (largely arbitrary) of the phase space, i.e. the choice of a symbolic sequence, thus not being invariant under smooth coordinate transformations. On the other hand, the calculation of generalized dimensions (which are invariant) closely related to these entropies is free from such conventions. The results of the present paper show that the correlation dimension, which can be considered as a lower bound for the information dimension, behaves in a way similar to that of the local transport coefficients defined in [37], namely chaotic trajectory segments evolving close to regular regions of the phase space are forced to generate sets with lower values of $D^{(2)}$ than those segments evolving far away from such “quasi-barriers”. Evidently more work needs to be done in order to answer how the value of this dimension, but also other relevant quantities, is related to the time spent, or equivalently the local diffusion coefficient, in regions where motion is geometrically confined by layers of imperfect barriers.

Acknowledgements

We would like to thank Dr. H. Isliker for many useful and clarifying discussions on time series analysis and dimension estimate techniques, as well as for his critical comments on the first draft of this paper which helped us to improve the presentation. This work was completed while K.T. was under a grant from the State Scholarship Foundation of Greece (IKY). A.A. and K.T. would also like to acknowledge financial support by the PENED-95 programme Nr. 1857 of the Greek General Secretariat of Research and Technology.

References

- [1] Konishi T. Relaxation and diffusion in Hamiltonian systems with many degrees of freedom. *Progr Theoret Phys Suppl* 1989;98: 19–35.
- [2] Lecar M, Franklin F, Murison M. On predicting longterm orbital instability a relation between the Lyapunov time and sudden orbital transitions. *Astron J* 1992;104:1230–6.
- [3] Murison M, Lecar M, Franklin F. Chaotic motion in the outer asteroid belt and its relation to the age of the solar system. *Astron J* 1994;108:2323–9.
- [4] Morbidelli A, Froeschlé C. On the relationship between Lyapunov times and macroscopic instability times. *Celest Mech Dyn Astron* 1996;63:227–39.

- [5] Varvoglis H, Anastasiadis A. Transport in Hamiltonian systems and its relationship to the Lyapunov time. *Astron J* 1996; 111:1718–20.
- [6] Arnold VI. Instabilities of dynamical systems with many degrees of freedom. *Dokl Acad Nauk SSSR* 1964;196:9. English translation in *Soviet Math Dokl* 5:581.
- [7] Chirikov BV. A universal instability of many-dimensional oscillator systems. *Phys Rep* 1979;52:263–379.
- [8] Aubry S. The new concept of transitions by breaking of analyticity in a crystallographic model. In: Bishop AR, Schneider T, editors. *Solitons and condensed matter physics*. Series in Solid State Science no 8. New York: Springer, 1978. p. 264–77.
- [9] Percival IC. Variational principles for invariant tori and cantori. In: Month M, Herrera JC, editors. *Nonlinear dynamics and the beam beam interaction*. Woodbury, NY: American Institute of Physics, 1979. p. 302–10.
- [10] Varvoglis H, Vozikis Ch, Barbanis B. In: Hernard J, Dvorak R, editors. *The dynamical behaviour of our planetary system*. Dordrecht: Kluwer, 1997. p. 232–42.
- [11] Efthymiopoulos C, Contopoulos G, Voglis N, Dvorak R. Stickiness and cantori. *J Phys A* 1997;30:8167–86.
- [12] Contopoulos G, Polymilis C. Geometrical and dynamical properties of homoclinic tangles in a simple Hamiltonian system. *Phys Rev E* 1993;46:1546–57.
- [13] Shlesinger MF, Zaslavsky GM, Klafter J. Strange kinetics. *Nature* 1993;363:31–7.
- [14] Zaslavsky G. Fractional kinetic equation for Hamiltonian chaos. *Physica D* 1994;76:110–22.
- [15] Benzi R, Paladin G, Parisi G, Vulpiani A. *J Phys A* 1985;18:2157.
- [16] Froeschle C, Froeschle Ch, Lohinger E. Generalized Lyapunov indicators and corresponding Kolmogorov like entropy of the standard mapping. *Celest Mech Dyn Astron* 1993;56:307–15.
- [17] Voglis N, Contopoulos G. Invariant spectra of orbits in dynamical systems. *J Phys A* 1994;27:4899–909.
- [18] Kandrup HE, Eckstein BL, Bradley BO. Chaos complexity and short time Lyapunov exponents two alternative characterisations of chaotic orbit segments. *Astron Astrophys* 1997;320:65–73.
- [19] Froeschle C, Lega E, Gonczi R. Fast Lyapunov indicators. Application to asteroidal motion. *Celest Mech Dyn Astron* 1997;67:41–62.
- [20] Eykholt R, Umberger DK. Characterization of fat fractals in nonlinear dynamical systems. *Phys Rev Lett* 1986;57:2333–6.
- [21] Magneat P. Numerical study of periodic orbit properties in a dynamical system with three degrees of freedom. *Celest Mech* 1982;28:319–43.
- [22] Contopoulos G, Barbanis B. Lyapunov characteristic numbers and the structure of phase-space. *Astron Astrophys* 1989;222: 329–43.
- [23] Contopoulos G, Barbanis B. Order in the distribution of 3-D periodic orbits. *Astron Astrophys* 1995;294:33–46.
- [24] Press WH, Teukolsky SA, Vetterling WT, Flannery BP. *Numerical recipes in Fortran – The art of scientific computing*. 2nd ed. Cambridge: Cambridge University Press, 1992.
- [25] Lichtenberg AJ, Leiberman MA. *Regular and stochastic motion*. New York: Springer, 1983.
- [26] Takens F. Detecting strange attractors in turbulence. *Lecture Notes in Math*. 1981;898:366–81.
- [27] Sauer T, Yorke J, Casdagli M. *Embedology*. *J Stat Phys* 1991;65:579–616.
- [28] Isliker H. *Dynamical properties of bursts and flares: An inquiry on deterministic chaos in the solar and stellar coronae*. PhD Thesis, ETH: No 10495, Swiss Federal Institute of Technology, Zürich, 1994.
- [29] Tsonis A. *Chaos. From theory to applications*. New York: Plenum Press, 1992.
- [30] Isliker H. A scaling test for correlation dimensions. *Phys Lett A* 1992;169:313–22.
- [31] Kantz H, Schreiber T. In: Chirikov B, Cvitanović P, Moss F, Swinney H, editors. *Nonlinear time series analysis*. Cambridge nonlinear science series 7, Cambridge: Cambridge University Press, 1997.
- [32] Isliker H, Kurths J. A test for stationarity finding parts in time series apt for correlation dimension estimates. *Int J Bifurc Chaos* 1993;3:1573–9.
- [33] Ellner S. Estimating attractor dimensions from limited data – a new method with error estimates. *Phys Lett* 1988;133A:128–33.
- [34] Varvoglis H, Voyatzis G, Scholl H. Spectral analysis of asteroidal trajectories in the 2:1 resonance. *Astron Astrophys* 1995;300:591–6.
- [35] Milani A, Nobili AM. An example of stable chaos in the solar system. *Nature* 1992;357:569–71.
- [36] Milani A, Nobili AM, Knezevic Z. Stable chaos in the asteroid belt. *Icarus* 1997;125:13–31.
- [37] Yannacopoulos AN, Rowlands G. Local transport coefficients for chaotic systems. *J Phys A* 1997;30:1503–25.
- [38] Benkadda S, Elskens Y, Ragot B. *Phys Rev Lett* 1994;72:2859.
- [39] Tsiganis K, Varvoglis H, Hadjidemetriou JD. Stable chaos in the 12:7 mean motion resonance and its relation to the stickiness effect. *Icarus* 1999, submitted.